Supporting Information

Schuhmacher et al. 10.1073/pnas.1419388112

SI Materials and Methods

Plasmids. Genes encoding for the proteins used in this study were amplified from genomic DNAs of *B. subtilis* PY79, *G. thermodenitrificans* NG80-2, and *S. putrefaciens* CN-32 by PCR using Q5 High-Fidelity DNA polymerase (New England Biolabs) according to the manufacturer's manual. Primers were designed according to the following gene annotations: *B. subtilis* PY79: U712_08620 (*flhG*), U712_08570 (*fliM*), and U712_08575 (*fliY*); *G. thermodenitrificans* NG80-2: GTNG_1094 (*flhG*), GTNG_1083 (*fliM*), GTNG_1084 (*fliY*;; GTNG_1073 (*fliG*), and GTNG_2544 (*minC*); and *S. putrefaciens* CN-32: Sputcn32_2560 (*flhG*), Sputcn32_2569 ($fliM_1$), Sputcn32_2568 ($fliN_1$), Sputcn32_3479 ($fliM_2$), and Sputcn32_3480 ($fliN_2$). A protocol for isolating *S. putrefaciens* CN-32 genomic DNA was described previously (1). A $(His)_6$ tag was encoded in either the forward or reverse primer. The PCR fragment was cloned into pET24d(+) or pET16b vectors (Novagen) via commonly used restriction sites (i.e., *NcoI*/*PciI*/*BamHI*/*XhoI*). Enzymes used in this study were purchased from New England Biolabs, Biozym Scientific GmbH, and Fermentas. Mutations within FlhG were generated using QuikChange II site-directed mutagenesis (Agilent). The FlhG-YFP fusion was made by cloning the last 500 coding base pairs of *flhG* (*ylxH* gene) into the plasmid pSG1164 (2). Constructions of markerless in-frame deletion or integration mutants in *S. putrefaciens* CN-32 based on the suicide vector pNPTS138-R6KT were performed as described previously (3, 4). Amino acid substitutions in FlhG were introduced by appropriate codon modifications in *flhG* and reintegration into a Δ*flhG* mutant. Production and stability of the FlhG variants were confirmed by Western immunoblotting. To construct $FliM_1$-ΔNtr, the sequence corresponding to amino acid positions 2–28 was deleted in $fliM_1$ in the background strains. Western immunoblotting and fluorescence microscopy confirmed the stable production of the mCherry-labeled proteins. To enable fluorescence labeling of $FlgE_2$, an ACC-to-TGC codon substitution was introduced into $flgE_2$, yielding a Thr242Cys substitution ($FlgE_{2\text{-}Cys}$). The modified gene was reintroduced into the corresponding Δ$flgE_2$ mutant of *S. putrefaciens* CN-32. The substitution did not affect the motility of the resulting mutant as determined by soft-agar assays (Fig. S6*E*) and light microscopy.

Strains, Growth Conditions, and Media. All strains used and constructed in this study are summarized in Table S2. In *B. subtilis*, FlhG-YFP fusion protein is expressed from the original genetic locus, and a xylose-inducible promotor controls downstream genes. For colocalization studies, a strain expressing FliM-CFP from the ectopic *amyE* locus (a kind gift of Daniel B. Kearns, Indiana University, Bloomington, IN) was transformed with chromosomal DNA of the FlhG-YFP strain. Functionality of FliM-CFP fusion has been demonstrated in the literature (5). The functionality of FlhG was verified intrinsically by coexpression with FliM-CFP, because defective FlhG would have led immediately to aberrant FliM foci, which were not observed (5). *E. coli* strains DH5α λpir, BL-21, and WM3064, *B. subtilis* strain PY 79, and *S. putrefaciens* CN-32 were grown routinely in lysogeny broth (LB) medium at 37 °C and 30 °C, respectively. The medium for the 2,6-diaminopimelic acid (DAP)-auxotroph *E. coli* WM3064 was supplemented with DAP at a final concentration of 300 μM. To solidify media, LB agar was prepared using 1.5% (wt/vol) agar. When required, media were supplemented with 100 μg/mL ampicillin, 50 μg mL kanamycin, and/or 10% (wt/vol) sucrose. To prepare agarose pads for fluorescence microscopy, PBS (137 mM NaCl, 2.7 mM KCl, 10 mM Na_2HPO_4, 1.8 mM KH_2PO_4, pH 7.4) was solidified by adding 1% (wt/vol) agarose. *B. subtilis* strains were plated onto LB-agar plates containing 0.5% xylose and the respective antibiotics. The strains used in this study are listed in Table S2.

Protein Production and Purification. For gene expression, *E. coli* BL21 (DE3) were grown in LB medium under autoinduction conditions [D(+)-lactose-monohydrate, 1.75% (wt/vol)] supplemented with the respective antibiotics (50 μg/mL kanamycin or 100 μg/mL ampicillin) at 30 °C for ∼16 h under constant shaking (150 rpm). Cells were harvested by centrifugation (4,000 rpm/3,500 × *g* for 20 min at 4 °C), suspended in lysis buffer [20 mM Hepes-Na (pH 8.0), 250 mM NaCl, 40 mM imidazole, 20 mM $MgCl_2$, and 20 mM KCl] and subsequently lysed using the M-110L Microfluidizer (Microfluidics). After centrifugation (23,000 rpm/63,000 × *g* for 20 min at 4 °C), the clarified lysate was applied to a 1-mL HisTrap FF column (GE Healthcare) equilibrated with 10 column volumes of lysis buffer. After washing with 70 mL lysis buffer, proteins were eluted using 15 mL elution buffer (lysis buffer containing 500 mM imidazole). Elution fractions containing protein were concentrated using Amicon Ultracel-10K (Millipore) and subsequently applied to SEC (HiLoad 26/600 Superdex 200 pg, GE Healthcare) equilibrated in SEC buffer [20 mM of Hepes-Na (pH 7.5), 200 mM NaCl, 20 mM $MgCl_2$, and 20 mM KCl]. Fractions were analyzed using SDS/PAGE. Protein containing fractions were pooled and concentrated according to experimental requirements. Concentration was determined by a spectrophotometer (NanoDrop Lite; Thermo Scientific). FliM and FliY were coexpressed and copurified via a $(His)_6$ tag at the C terminus of FliM. A trimeric complex containing FliM, FliY, and FlhG was copurified using two His tags at the C terminus of FliM and the N terminus of FlhG.

Crystallization of *Gt*FlhG. All crystallization experiments were carried out by the sitting-drop method in SWISSCI MRC two-well crystallization plates at room temperature. The reservoir volume was 50 μL, and the drop volume was 1 μL, with a 1:1 mixture of protein and crystallization solution. Crystals of apo-*Gt*FlhG were obtained from a 20.0 mg/mL solution after ∼3 wk in 0.1 M Hepes (pH 7.5), 10% (wt/vol) PEG 8000, 0.1 urea. Crystals of the dimeric state of FlhG were obtained from a 20.0 mg/mL solution of the *Gt*FlhG D60A variant after ∼3 wk in a buffer containing 0.1 M Hepes (pH 7.0) and 20% (wt/vol) PEG 6000. Before crystallization, FlhG-D60A was incubated with 4.4 mM ATP for 1 h on ice.

Data Collection, Structure Determination, and Analysis. Before data collection, crystals were flash-frozen in liquid nitrogen after a short incubation in a cryo-protecting solution that consisted of mother liquor supplemented with 20% (vol/vol) glycerol. Data collection was performed at the European Synchrotron Radiation Facility in Grenoble, France under cryogenic conditions beamlines: ID 23-2 (apo-state of FlhG) and ID 23-1 (dimeric state of FlhG). Data were recorded with a DECTRIS PILATUS 6M detector. Data were processed using iMosflm (6) and the CCP4-implemented program SCALA (7). The structure of apo-FlhG was solved by molecular replacement with CCP4-integrated PHASER (8) using *Ec*MinD (PDB ID code: 3QL9) and monomeric FlhG (this study) as search models. Structures were built manually in COOT (9) and were refined using PHENIX refine (10). Figures were designed with PyMol (www.pymol.org).

HDX Mass Spectroscopy. HDX experiments were performed as described previously (11–13). Minor adjustments of the setup mainly concerned the HPLC pumps (isocratic: 1100 series; Agilent Technologies/Hewlett Packard; gradient: 1260 Infinity; Agilent Technologies) and the mass analyzer (Orbitrap Velos Pro; Thermo Scientific). Purified and concentrated *Gt*FlhG and *Gt*FliY, and the *Gt*FlhG-FliY complex (200 pmol, 50 μM) were diluted 10-fold into D_2O-containing SEC buffer [20 mM Hepes (pH 7.5), 200 mM NaCl, 20 mM KCl, and 20 mM $MgCl_2$] and were incubated at 37 °C to start H/D exchange. After 30 s the reaction was quenched by decreasing the temperature to 0 °C and adding one equivalent (50 μL) of Quench buffer [400 mM KH_2PO_4/H_3PO_4 (pH 2.2)]. The samples were injected immediately onto HPLC. Peptic peptides from the on-line digest were analyzed directly by mass spectrometry, and the deuterium content was calculated using HDX workbench (14). Relative deuteron incorporation was calculated based upon the centroids of the molecular ion isotope distribution extracted from the software. For adjustment, the 0% control was treated with H_2O buffer. Complete exchange was defined as 90% of the possible incorporation and applied to all samples, because of dilution and re-exchange during the HPLC run.

GST-Binding Assays. GST pulldown assays were performed in PBS buffer at 4 °C. Purified GST-protein (i.e., GST-FlhG, GST-FliG) (1 nmol) was applied to 15 μL glutathione Sepharose 4B (GE Healthcare) in small filter columns (MoBiTec) by incubation on a wheel for 15 min. Subsequently, 2 nmol of putative binding partners (i.e., FlhG, FliY, FliM) and 2.5 mM of appropriate nucleotides were added and incubated for 10 min at 4 °C on the wheel. After centrifugation [4,000 rpm (3,500 × *g*), for 1 min at 4 °C] the column was washed three times with PBS buffer. Proteins were eluted with 40 μL of GSH buffer [50 mM Tris·HCl, 20 mM GSH (pH 7.5)] and analyzed by Coomassie-stained SDS/PAGE. Conditions for time-resolved GST pulldown assays were adjusted toward physiological temperature (37 °C) and carried out using SEC-buffer.

Ni-NTA Affinity Binding Assays. FlhG variants were investigated for their ability to bind FliM/FliY by Ni-NTA affinity pulldown assays from expression cultures. Expression culture of $(His)_6$-tagged FlhG variants (100 mL) and untagged FliM/FliY coexpression were mixed, harvested, and lysed as stated (*Protein Production and Purification*). Ni-NTA agarose (300 μL) (Qiagen) was added to the clarified lysate and incubated for 15 min on ice. After centrifugation (4,000 rpm/3,500 × *g* for 15 min at 4 °C), the lysate was discarded, and the loaded Ni-NTA agarose was washed three times with 500 μL of lysis buffer and subsequently was centrifuged (4,000 rpm/3,500 × *g* for 5 min at 4 °C). Proteins were eluted with 300 μL of elution buffer and were analyzed by Coomassie-stained SDS/PAGE.

Fluorescence Microscopy. *B. subtilis* cells were cultivated in LB medium at 37 °C to exponential growth phase (OD_{600} 0.5) and were immobilized on coverslips by $S7_{50}$ medium containing agarose pads (1% wt/vol). Fluorescence microscopy was performed on a fully automated Leica SP 8 laser scanning microscope equipped with a 100× HCX PL APO STED objective (NA 1.4), an argon ion laser source, and Leica HyD detectors. Images were analyzed using the Huygens (Scientific Volume Imaging) and LAS AF (Leica) software. Foci that were immobile within the resolution limit (250 nm) for more than 5 s were defined as static.

Shewanella strains were cultured to midexponential phase before imaging. Appropriately diluted cultures (2–5 μL) were added on top of an agar pad to immobilize cells. A DMI6000 B fluorescence microscope (Leica) equipped with a HCX PL APO 100×/1.4 differential interference contrast (DIC) objective was used to visualize single cells. Image acquisition and processing were carried out using the VisiView Premier software (Visitron Systems GmbH) and ImageJ 1.47v software (National Institutes of Health) (15).

Hydrolysis Assays. The ATPase activity was investigated using an HPLC-based assay. FlhG, its D60A variant, and FliG were diluted to 20 μM (1 nmol) and supplemented with 2 mM ATP (100 nmol) and 25 μL of *E. coli* lipid vesicles. Hydrolysis assays were performed in SEC buffer at 37 °C with an incubation time of 1 h. Subsequent flash freezing in liquid nitrogen stopped the hydrolysis reaction. HPLC measurements were performed with an Agilent 1100 Series HPLC system (Agilent Technologies) and a C18 column (EC 250/4.6 Nucleodur HTec 3 μm; Macherey-Nagel). The samples were injected onto HPLC and run for 30 min with a buffer containing 50 mM KH_2PO_4, 50 mM K_2HPO_4, 10 mM TPAB, and 15% (vol/vol) acetonitrile at flow rate of 0.8 mL/min. ADP and ATP were detected by UV light at 260.8 nm and were quantified (by peak area) using ChemStation (B.04.03).

Flotation Assays. PE and PG were supplied by Avanti Polar Lipids. Lipids were mixed in ratio of 70% PE:30% PG, and the chloroform was evaporated under reduced pressure for 30 min. LUVs were prepared in assay buffer [100 mM phosphate, 750 mM NaCl, 10 mM $MgCl_2$, 1.2 M sucrose (pH 7.5)] by extrusion (16). After 10 freeze–thaw cycles, lipids were passed 21 times through a 100-nm pore polycarbonate filter (Nuclepore) in a two-syringe extruder (Avanti Polar Lipids), resulting in LUVs. Proteins were mixed with 50 μL of the LUV solution and were incubated for 20 min. Flotation gradient centrifugation was performed as described previously (17). Samples were mixed with 360 μL of assay buffer containing 50% iodixanol, overlaid with 1.16 mL of assay buffer with 30% iodixanol, and finally overlaid by 450 μL of assay buffer. After ultracentrifugation (Beckmann Coulter) for 3 h at 45,000 rpm (217,000 × *g*) in a swing-out rotor (MLS 50; Beckmann Coulter), the gradient was collected in three fractions (600 μL top, 800 μL middle, 600 μL bottom) and analyzed by SDS/PAGE after TCA precipitation. Briefly, the separated fractions were treated with 100 μL TCA and were incubated overnight at −20 °C. After centrifugation (Heraeus Fresco 17; Thermo Scientific) for 20 min at 13,000 rpm (16,200 × *g*) and 4 °C, the pellets were washed twice with 500 μL chilled acetone. Before SDS/PAGE analysis, the remaining acetone was evaporated (2 min at 95 °C).

Flagellar Staining. Staining of flagellar filaments was performed as described earlier (18). Ten microliters of an exponentially growing culture were spotted onto a microscopy slide and stained before visualization. Microscopy and image acquisition were carried out with a Leica DMI6000B microscope equipped with an HCX PL APO 100×/1.4 DIC objective.

Immunoblot Analysis. To determine production and stability of proteins, lysates from exponentially growing LB cultures were obtained for Western blot analyses. Subsequent to harvesting by centrifugation, cells corresponding to an OD_{600} of 10 were resuspended in sample buffer (19), heated at 99 °C for 5 min, and stored at −20 °C. Ten microliters of sample were resolved by SDS/PAGE using 11% polyacrylamide gels. Subsequently, proteins were transferred to PVDF Immobilon-P membrane (Millipore) through semidry transfer. To detect the fusion proteins, polyclonal antibodies raised against mCherry (Biovision Life Sciences), GFP (Roche GmbH) or purified *Sp*FlhG (in dilutions of 1:10,000, 1:5,000, and 1:1,000, respectively) were used. Secondary anti-rabbit IgG-HRP antibody was used at a dilution of 1:20,000 to detect mCherry and She-FlhG antibodies. For Roche GFP antibodies, a secondary anti-mouse IgG-alkaline phosphatase antibody was used at a dilution of 1:15,000. Signals were detected using the SuperSignal West Pico Chemiluminescent

Substrate (Thermo Scientific) or CDP-Star chemiluminescent substrate (Roche Diagnostics) and were documented using the CCD System Fusion SL4 (PEQLAB Biotechnologie).

Motility Assays. Spreading of *S. putrefaciens* CN-32 wild-type or mutant cell cultures was monitored by light microscopy or on soft-agar plates using previously established protocols (4, 20). Soft-agar plates had an agar concentration of 0.25% (wt/vol); 3 μL of an exponentially growing planktonic culture of the appropriate strain was spotted for a motility assay. The plates were incubated for an adequate amount of time at 30 °C, and the radial extension of the cultures was documented. To compare the radial extension of different mutant strains with that of wild-type *S. putrefaciens* CN-32, the appropriate cultures always were spotted onto the same soft-agar plate.

Fluorescence Staining of $FlgE_{2\text{-}Cys}$. Fluorescence coupling of $FlgE_{2\text{-}Cys}$, as a marker for intact secondary lateral flagella, was carried out essentially according to a previously published protocol (21, 22) with several modifications. One milliliter of a culture of the appropriate strain at 0.5 OD_{600} was pelleted and resuspended in 50 μL PBS buffer containing 5 μg/mL Alexa Fluor 488 C_5 maleimide (Molecular Probes), followed by incubation for 5 min at room temperature. Subsequently, cells were pelleted again and resuspended in 500 μL PBS. For fluorescence microscopy, 5 μL of the suspension was put on top of an agarose pad.

Transmission Electron Microscopy. To prepare samples for electron microscopy according to the methods described in ref. 4, cells were grown to midexponential phase. Glutaraldehyde was added to a final concentration of 1.25% (vol/vol) to fix cells for 15 min before washing once with lactate medium (LM) (10 mM Hepes, pH 7.5; 200 mM NaCl; 0.02% yeast extract; 0.01% peptone; 15 mM lactate). After washing, cells were concentrated via centrifugation at 13,000 rpm. The resulting pellet was suspended in 50 μL of medium, and 5 μL of the cell suspension was applied to glow-discharged and carbon-coated copper grids (400 square mesh; Plano). The samples were washed immediately twice with ddH_2O and were negatively stained with uranyl acetate (2%) for 20 s. Electron microscopy was performed on a JEOL 2100 TEM (JEOL Ltd.) equipped with a LaB_6 cathode and operated at 120 kV. To record images, a fast-scan 2 × 2k camera F214 combined with the EM-Menu 4 software (TVIPS) was used.

1. Pospiech A, Neumann B (1995) A versatile quick-prep of genomic DNA from gram-positive bacteria. *Trends Genet* 11(6):217–218.
2. Lewis PJ, Marston AL (1999) GFP vectors for controlled expression and dual labelling of protein fusions in *Bacillus subtilis*. *Gene* 227(1):101–110.
3. Lassak J, Henche AL, Binnenkade L, Thormann KM (2010) ArcS, the cognate sensor kinase in an atypical Arc system of *Shewanella oneidensis* MR-1. *Appl Environ Microbiol* 76(10):3263–3274.
4. Bubendorfer S, et al. (2012) Specificity of motor components in the dual flagellar system of *Shewanella putrefaciens* CN-32. *Mol Microbiol* 83(2):335–350.
5. Guttenplan SB, Shaw S, Kearns DB (2013) The cell biology of peritrichous flagella in *Bacillus subtilis*. *Mol Microbiol* 87(1):211–229.
6. Battye TGG, Kontogiannis L, Johnson O, Powell HR, Leslie AGW (2011) iMOSFLM: A new graphical interface for diffraction-image processing with MOSFLM. *Acta Crystallogr D Biol Crystallogr* 67(Pt 4):271–281.
7. Winn MD, et al. (2011) Overview of the CCP4 suite and current developments. *Acta Crystallogr D Biol Crystallogr* 67(Pt 4):235–242.
8. McCoy AJ, et al. (2007) Phaser crystallographic software. *J Appl Cryst* 40(Pt 4):658–674.
9. Emsley P, Cowtan K (2004) Coot: Model-building tools for molecular graphics. *Acta Crystallogr D Biol Crystallogr* 60(Pt 12 Pt 1):2126–2132.
10. Adams PD, et al. (2010) PHENIX: A comprehensive Python-based system for macromolecular structure solution. *Acta Crystallogr D Biol Crystallogr* 66(Pt 2): 213–221.
11. Rist W, Jørgensen TJ, Roepstorff P, Bukau B, Mayer MP (2003) Mapping temperature-induced conformational changes in the *Escherichia coli* heat shock transcription factor sigma 32 by amide hydrogen exchange. *J Biol Chem* 278(51):51415–51421.
12. Stjepanovic G, et al. (2011) Lipids trigger a conformational switch that regulates signal recognition particle (SRP)-mediated protein targeting. *J Biol Chem* 286(26):23489–23497.
13. Kressler D, et al. (2012) Synchronizing nuclear import of ribosomal proteins with ribosome assembly. *Science* 338(6107):666–671.
14. Pascal BD, et al. (2012) HDX workbench: Software for the analysis of H/D exchange MS data. *J Am Soc Mass Spectrom* 23(9):1512–1521.
15. Schneider CA, Rasband WS, Eliceiri KW (2012) NIH Image to ImageJ: 25 years of image analysis. *Nat Methods* 9(7):671–675.
16. Hope MJ, Bally MB, Webb G, Cullis PR (1985) Production of large unilamellar vesicles by a rapid extrusion procedure: Characterization of size distribution, trapped volume and ability to maintain a membrane potential. *Biochim Biophys Acta* 812(1):55–65.
17. Parlitz R, et al. (2007) *Escherichia coli* signal recognition particle receptor FtsY contains an essential and autonomous membrane-binding amphipathic helix. *J Biol Chem* 282(44):32176–32184.
18. Heimbrook ME, Wang WL, Campbell G (1989) Staining bacterial flagella easily. *J Clin Microbiol* 27(11):2612–2615.
19. Laemmli UK (1970) Cleavage of structural proteins during the assembly of the head of bacteriophage T4. *Nature* 227(5259):680–685.
20. Bubendorfer S, Koltai M, Rossmann F, Sourjik V, Thormann KM (2014) Secondary bacterial flagellar system improves bacterial spreading by increasing the directional persistence of swimming. *Proc Natl Acad Sci USA* 111(31):11485–11490.
21. Blair KM, Turner L, Winkelman JT, Berg HC, Kearns DB (2008) A molecular clutch disables flagella in the *Bacillus subtilis* biofilm. *Science* 320(5883):1636–1638.
22. Courtney CR, Cozy LM, Kearns DB (2012) Molecular characterization of the flagellar hook in *Bacillus subtilis*. *J Bacteriol* 194(17):4619–4629.

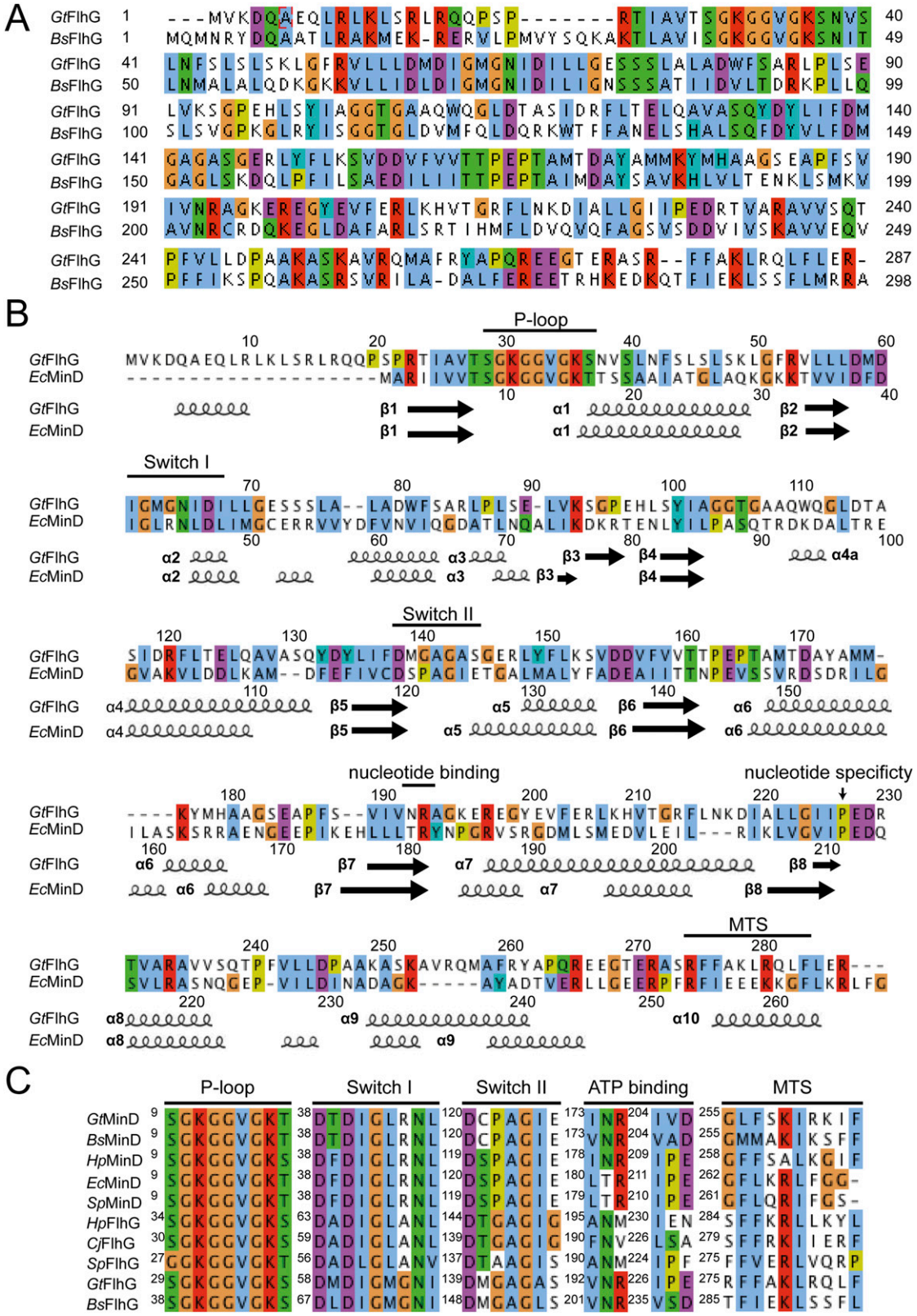

Fig. S1. Sequence and secondary structure alignments. (*A*) The color code indicates conservation and identity of amino acids between the FlhG homologs of *B. subtilis* and *G. thermodenitrificans*. (*B*) Alignment of *Gt*FlhG and *Ec*MinD shows the similarity of these ATPases. Secondary structure elements and important catalytic regions are indicated. *Ec*, *Escherichia coli*; *Gt*, *Geobacillus thermodenitrificans*. (*C*) FlhG and MinD share the catalytically important regions for ATP/magnesium binding and ATP hydrolysis: P-loop, Switch regions I and II, ATP-binding residues and a C-terminal, amphipathic helix. *Bs*, *Bacillus subtilis*; *Cj*, *Campylobacter jejuni*; *Ec*, *Escherichia coli*; *Gt*, *Geobacillus thermodenitrificans*; *Hp*, *Helicobacter pylori*; *Sp*, *Shewanella putrefaciens*.

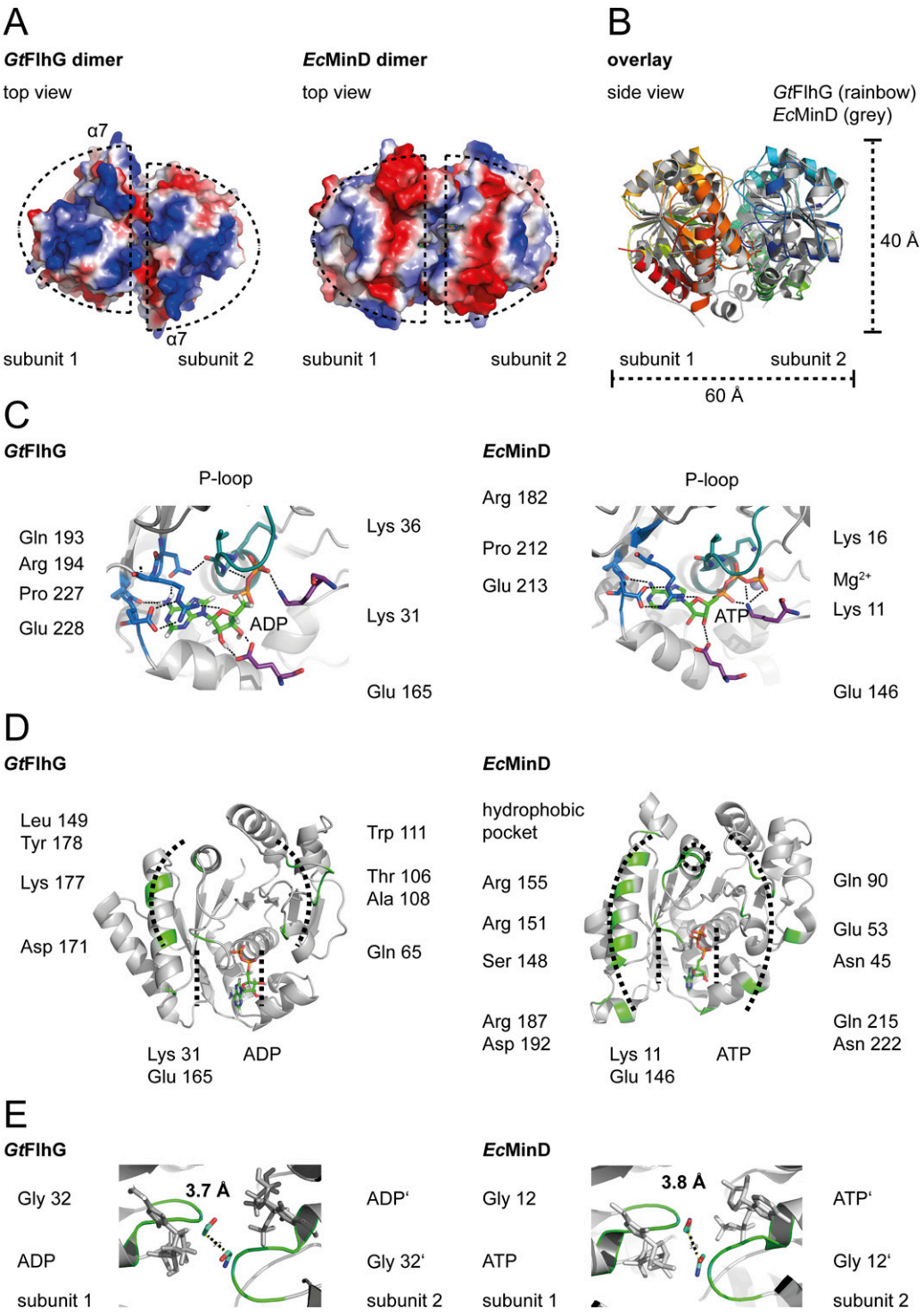

Fig. S2. Detailed structural analysis of the FlhG dimer. (*A*) Electrostatic surface views of the *Gt*FlhG (*Left*) and *Ec*MinD (*Right*) homodimers. The half-sites of each the homodimers are indicated by dashed lines. A protrusion caused by the extension of helix α7is visible in the FlhG homodimer. (*B*) Superimposition of the FlhG and MinD homodimers shown in rainbow color and gray, respectively. The dashed lines indicate approximate dimensions in angstroms. (*C*) A comparison of the active site of FlhG (*Left*) and MinD (*Right*) shows high structural resemblance and conservation of important residues. (*D*) The dimerization interface is larger in MinD than in FlhG (MinD: ∼1,100 Å^2; FlhG: ∼700 Å^2). Important elements are colored in green. Dashed lines represent the interaction interface. (*E*) The space between the subunits in FlhG (3.7 Å, *Left*) and MinD (3.8 Å, *Right*) is similar and was measured as the distance between conserved glycine residues (indicated as sticks) in the P-loop.

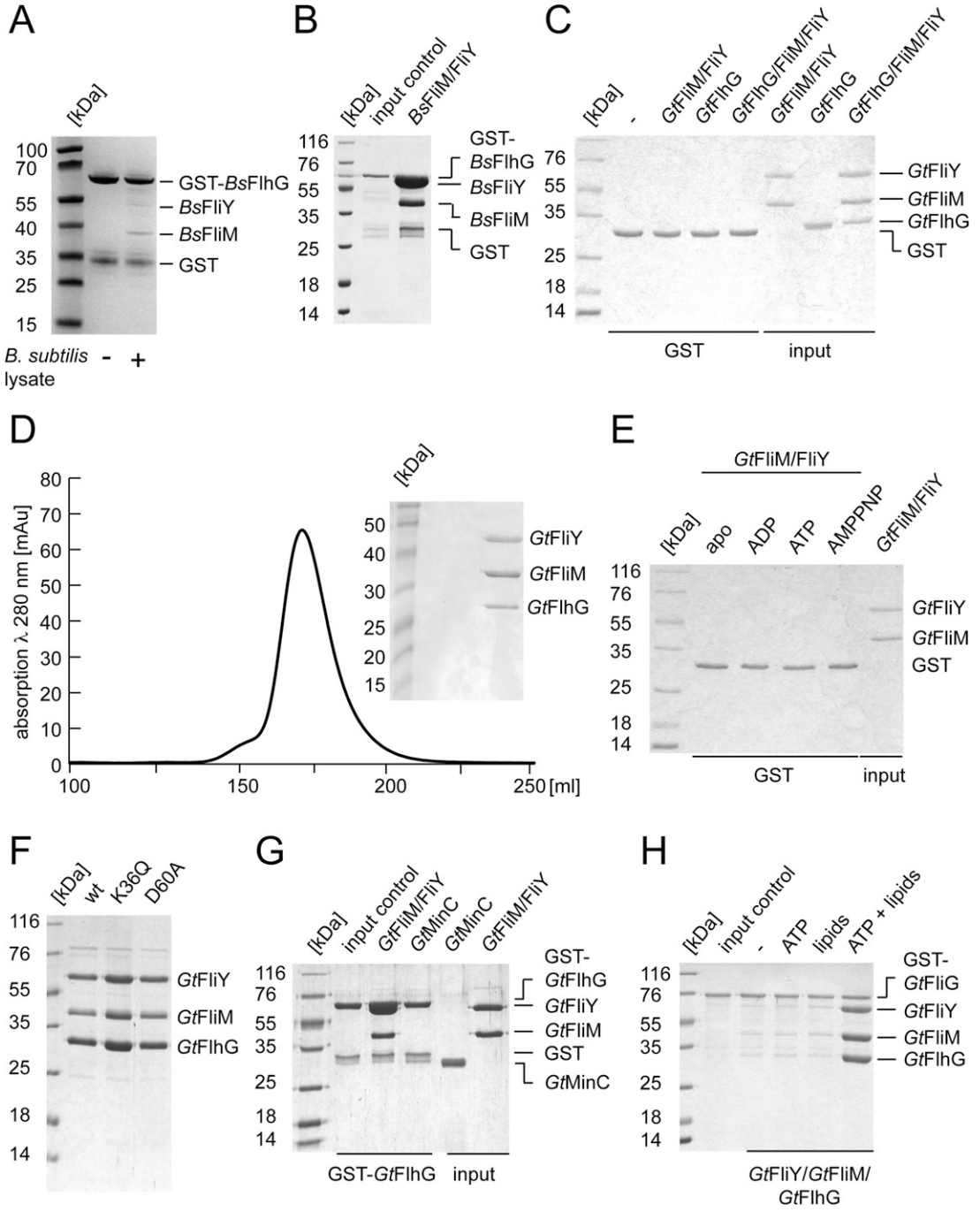

Fig. S3. FlhG binds FliM/FliY independent of nucleotides. (*A*) SDS/PAGE of an in vitro pulldown assay from whole-cell lysate of *B. subtilis* using GST-*Bs*FlhG. Mass spectrometry identified the potential interaction partners FliM and FliY. (*B*) Coomassie-stained SDS/PAGE of an in vitro pulldown assay demonstrates that GST-*Bs*FlhG (input control) interacts directly with *Bs*FliM/FliY. (*C*) In vitro pulldown assays using GST show that a *Gt*FliM/FliY complex, *Gt*FlhG, and a *Gt*FlhG/FliM/FliY complex do not interact with GST. Input controls are identified on the right. (*D*) Size-exclusion chromatogram of the *Gt*FliM/FliY/FlhG complex. (*Inset*) A Coomassie-stained SDS/PAGE of the peak fraction. (*E*) Coomassie-stained SDS/PAGE of the control pulldown assays reveals no unspecific interaction of a *Gt*FliM/FliY complex with GST in the presence of ADP, ATP, or AMPPNP. (*F*) In vitro pulldown assays show that two hydrolysis-deficient variants of *Gt*FlhG (K36Q and D60A) are as able to bind a *Gt*FliM/*Gt*FliY complex as the wild-type. (*G*) Coomassie-stained SDS/PAGE of an in vitro pulldown assay using GST-*Gt*FlhG. *Gt*MinC does not interact with GST-*Gt*FlhG, but the *Gt*FliM/FliY complex does. Input controls are shown in lanes 1 (GST-*Gt*FlhG), 4 (*Gt*MinC), and 5 (*Gt*FliM/FliY). (*H*) Coomassie-stained SDS/PAGE of an in vitro pulldown assay using GST-tagged *Gt*FliG incubated without (input control) and with *Gt*FliM/*Gt*FliY and *Gt*FlhG for 10 min. A stoichiometric ratio of FliM/FliY/FlhG exceeding 1 compared with GST-FliG was seen only in the presence of ATP and lipids.

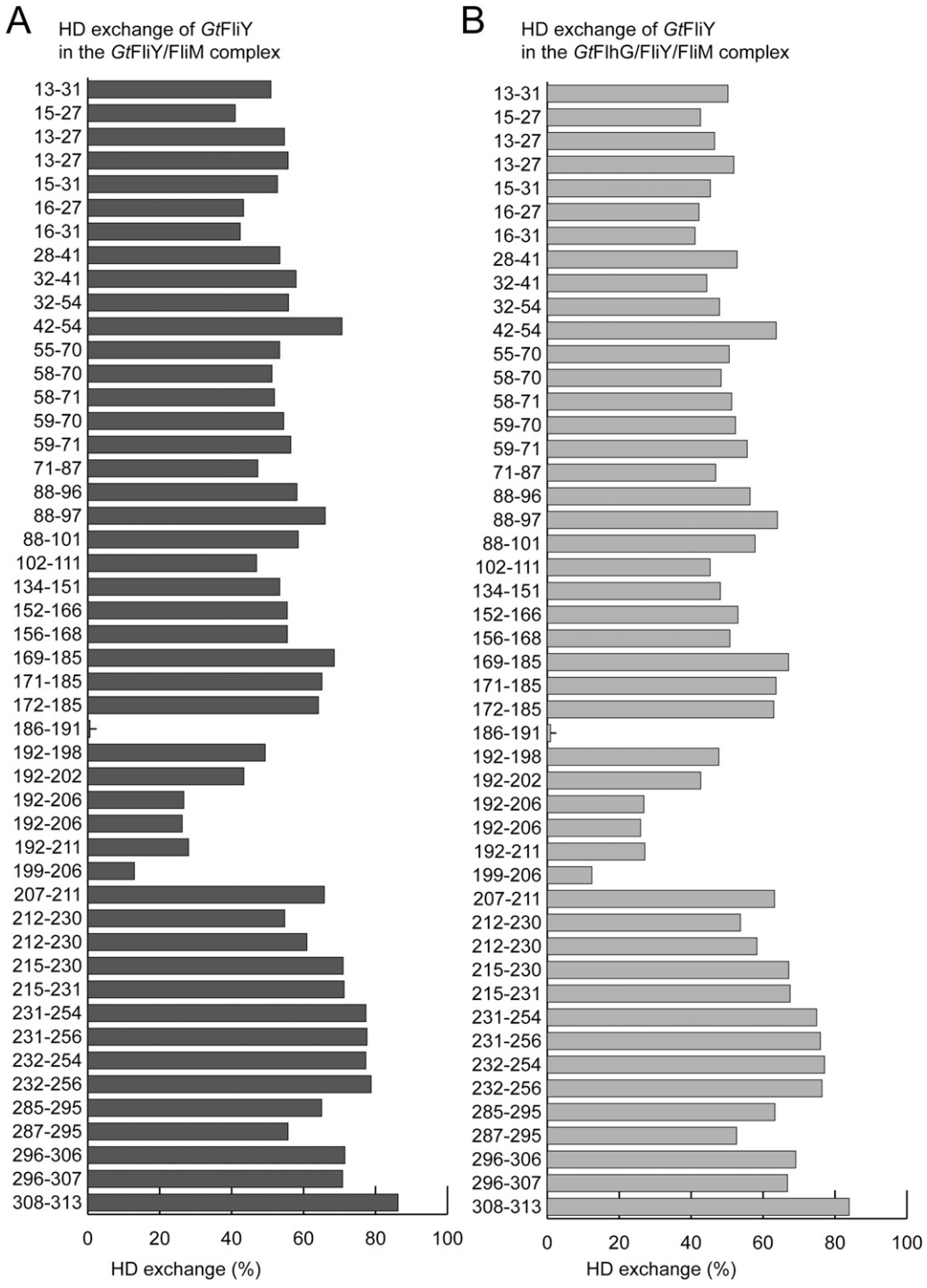

Fig. S4. Incorporation of deuterium into *Gt*FliY. (*A*) The percentage of deuterium incorporated into the peptic peptides of *Gt*FliY in a *Gt*FliM/FliY complex. (*B*) The deuterium content of the same peptic peptides from a *Gt*FlhG/FliY/FliM complex is displayed as percent (original mass spectrometric data are available on request to G.B.).

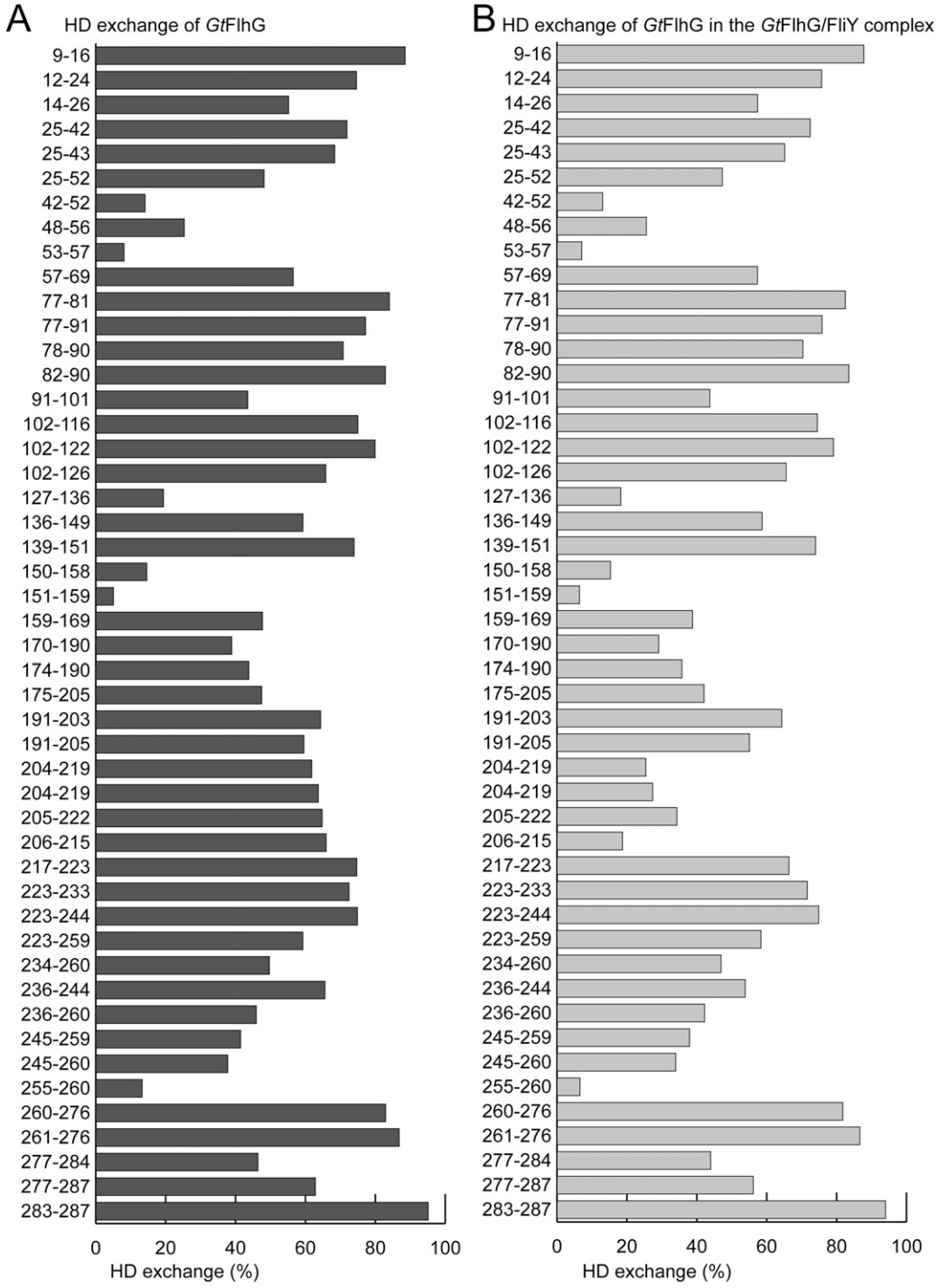

Fig. S5. Incorporation of deuterium into *Gt*FlhG. (*A*) The percentage of deuterium incorporated into *Gt*FlhG is shown for each peptide. (*B*) Incorporation of deuterium into peptic peptides obtained from a *Gt*FlhG/FliY complex is given as percent (original mass-spectrometric data are available on request to G.B.)

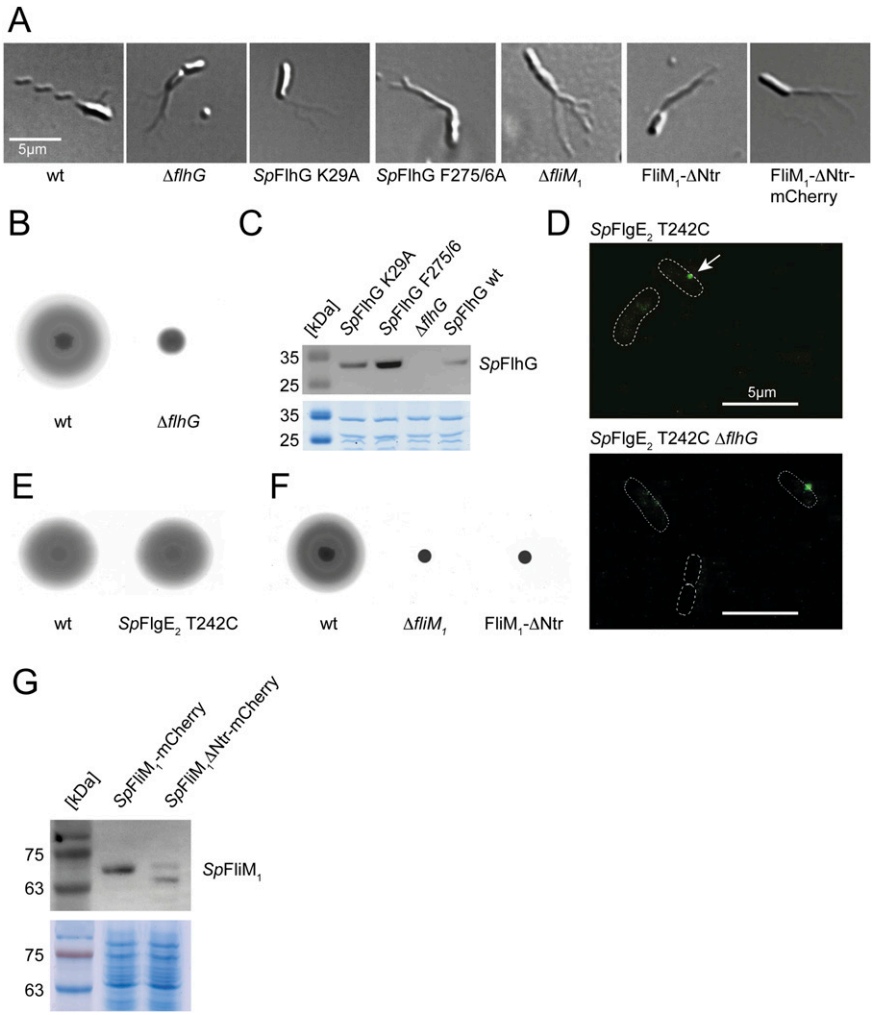

Fig. S6. Characteristics of FlhG from *S. putrefaciens*. (*A*) Flagella staining of various *flhG* and *fliM*$_1$ mutants in *S. putrefaciens* CN-32. Substitution mutants of *Sp*FlhG affecting membrane targeting (*Sp*FlhG F275/6A) and ATPase function (*Sp*FlhG K29A) display a hyperflagellation state similar to that of the *flhG* deletion mutant. *S. putrefaciens* mutant strains lacking the Ntr of FliM$_1$ (FliM$_1$-ΔNtr and FliM$_1$-ΔNtr-mCherry) show hyperflagellation similar to that of a *ΔfliM*$_1$ strain. (*B*) A soft-agar assay demonstrates that *Shewanella ΔflhG* mutants lack motility. (*C*) Western blot analysis shows the expression and stability of *Sp*FlhG and its variants K29A and F275/276A. In the Δ*flhG* strain of *S. putrefaciens,* no FlhG was observed. (*D*) Staining of the hook protein *Sp*FlgE$_2$ of the secondary lateral flagellum was performed as described, and the cells were used for fluorescence microscopy. Arrows point at clusters of FlgE$_2$, the hook protein of the lateral flagellar system, indicating the presence of a complete secondary flagellum. (*E*) A soft-agar assay demonstrates that the T242C substitution, which enables effective labeling, does not affect flagellar function. (*F*) Motility of *S. putrefaciens* (*Left*) and its *ΔfliM1* (*Center*) and *fliM1ΔNtr* (*Right*) mutant strains was monitored on swimming plates (0.25% agarose) at 30 °C. (*G*) Expression and protein integrity of *Sp*FliM$_1$-mCherry and its N-terminal deletion variant *Sp*FliM$_1$-ΔNtr-mCherry was verified by Western blot analysis.

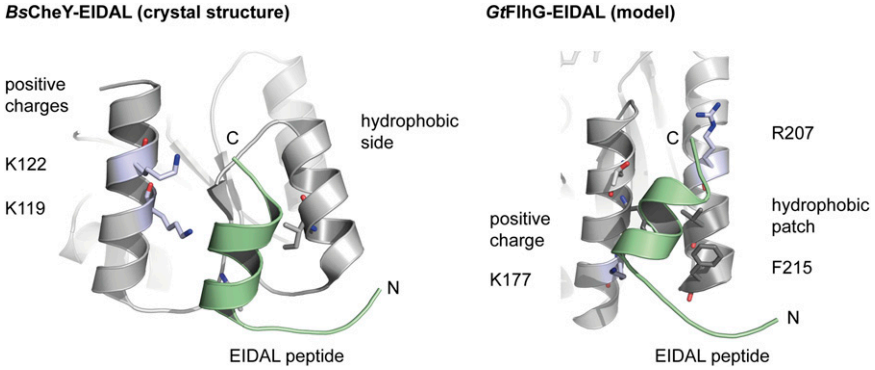

Fig. S7. Molecular mimicry. (*Left*) The interaction of *Bs*CheY with the EIDAL motif of *Bs*FliM from *B. subtilis* (PDB ID code: 2B1J). Important residues and characteristics of the interaction interface are depicted. (*Right*) The EIDAL motif in an arbitrary placement at the *Gt*FliY-binding site of *Gt*FlhG. Amino acid residues of FlhG, that are essential for binding of FliM/FliY as shown in this study, are highlighted. Note: The model of FlhG with the EIDAL peptide is intended to suggest size relationships rather than presenting a precise molecular model.

Table S1. Data collection and refinement

Data collection	*Gt*FlhG-monomer	*Gt*FlhG-dimer
Space group	P $2_12_12_1$	P 2_1
Cell dimensions		
a, *b*, *c*, Å	63.87	51.25
	89.36	72.56
	111.88	65.62
α, β, γ, °	90.00	90.00
	90.00	93.73
	90.00	90.00
Energy, keV	12.6616	
Resolution, Å	51.96–2.80	41.8–1.90
	(2.95–2.80)	(2.00–1.90)
R_{merge}	0.136 (0.47)*	0.058 (0.247)*
$I/\sigma I$	11.7 (5.2)	12.0 (5.8)
Completeness, %	100 (100)	99.2 (99.4)
Redundancy	5.1 (5.2)	3.9 (3.9)
Refinement		
Resolution, Å	47.4–2.80	29.84–1.90
No. reflections	15916	36165
R_{work}/R_{free}, %	17.7/22.8	22.1/26.0
No. atoms		
Protein	3,952	3,743
Ligand	0	38
Water	57	246
Rmsd		
Bond lengths, Å	0.008	0.008
Bond angles, °	1.228	1.229
Ramachandran, %		
Preferred	96.64	96.90
Allowed	3.12	2.69
Outliers	0.20	0.41

*Values in parentheses are for the highest-resolution shell.

Table S2. Description of bacterial strains

Bacterial strain	Relevant genotype or description	Source
Escherichia coli		
DH5α λpir	ϕ80dlacZ ΔM15 Δ(lacZYA-argF)U169 recA1 hsdR17 deoR thi-l supE44 gyrA96 relA1/λpir	(1)
WM3064	thrB1004 pro thi rpsL hsdS lacZ ΔM15 RP4 - 1360 Δ(araBAD) 567ΔdapA 1341::[erm pir(wt)]	W. Metcalf, University of Illinois at Urbana-Champaign, Urbana, IL
Shewanella putrefaciens		
CN-32	CN-32, wild-type	(2)
S 2576	Δ*flaAB*$_2$; markerless deletion of lateral flagellin genes *flaA*$_2$ and *flaB*$_2$ (Sputcn32_3455–Sputcn32_3456)	(3)
S 3133	Δ*flhG*, ΔSputcn32_2560; markerless deletion of the MinD-like ATPase FlhG	This study
S 3218	Δ*flaAB*$_2$ Δ*flhG*; markerless deletion of the *flhG* gene in the Δ*flaAB*$_2$ background	This study
S 3414	Δ*flgE*$_2$, ΔSputcn32_3465; markerless deletion of lateral flagellar hook protein	This study
S 3419	FlgE$_2$-T242C, markerless insertion of *flgE*$_2$ with substituted threonin 242 to cysteine into Δ*flgE*$_2$; used for fluorescence labeling of lateral flagellar hook proteins	This study
S 3470	Δ*flaAB*$_2$ Δ*flhG*; markerless deletion of *flhG* in the FlgE$_2$-T242C background	This study
S 3498	FliM$_1$-ΔNtr; markerless deletion of residues 2–28 of the polar motor protein FliM$_1$ (Sputcn32_2569)	This study
S 3523	FliM$_1$-ΔNtr-mCherry; markerless chromosomal fusion of FliM$_1$-ΔNtr to mCherry (C-terminal)	This study
S 3334	FlhG_F275AF276A, markerless insertion of *flhG* with substituted phenylalanine 275 to alanine and phenylalanine 276 to alanine into Δ*flhG*; disables the function of the membrane targeting sequence	This study
S 3335	FlhG_K29A, markerless insertion of *flhG* with substituted lysine 29 to alanine into Δ*flhG*; disables dimer formation and ATP hydrolysis	This study
S 3481	*flhG* KI; markerless insertion of *flhG* into Δ*flhG*; complements mutation	This study
S 3472	Δ*fliN*$_1$; markerless deletion of the polar C ring motor with protein FliN$_1$	This study
Bacillus subtilis		
PY79	PY79; wild-type	(4)
Jss01	PY79 *flhG-yfp* (Cm^R)	This study
Jss02	PY79 *flhG-yfp* (Cm^R) *amyE*::*fliM-cfp* (Spec^R)	This study

1. Miller VL, Mekalanos JJ (1988) A novel suicide vector and its use in construction of insertion mutations: Osmoregulation of outer membrane proteins and virulence determinants in *Vibrio cholerae* requires *toxR*. *J Bacteriol* 170(6):2575–2583.
2. Fredrickson JK, et al. (1998) Biogenic iron mineralization accompanying the dissimilatory reduction of hydrous ferric oxide by a groundwater bacterium. *Geochim Cosmochim Acta* 62(19–20):3239–3257.
3. Bubendorfer S, Koltai M, Rossmann F, Sourjik V, Thormann KM (2014) Secondary bacterial flagellar system improves bacterial spreading by increasing the directional persistence of swimming. *Proc Natl Acad Sci USA* 111(31):11485–11490.
4. Zeigler DR, et al. (2008) The origins of 168, W23, and other *Bacillus subtilis* legacy strains. *J Bacteriol* 190(21):6983–6995.

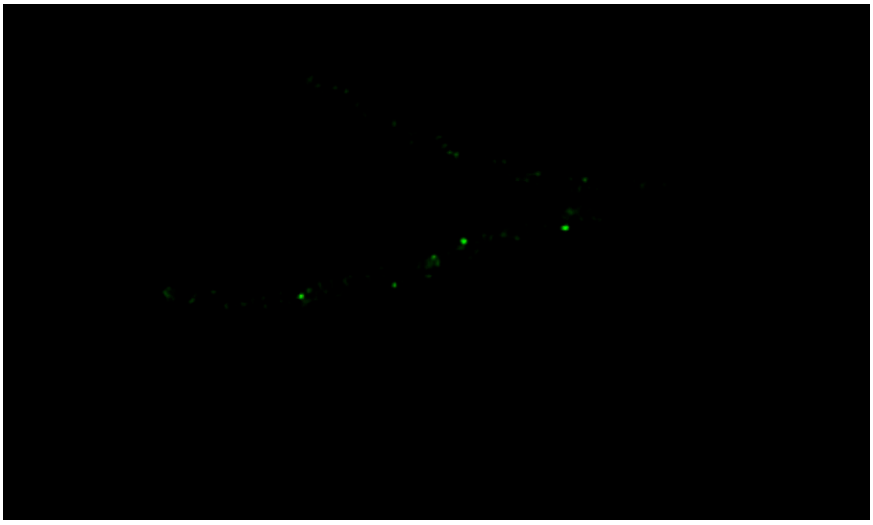

Movie S1. The dynamics of *Bs*FlhG-YFP in *B. subtilis* were followed over 30 s. Images were acquired every 3.24 s and are displayed with a frame rate of three frames/s.

Movie S1

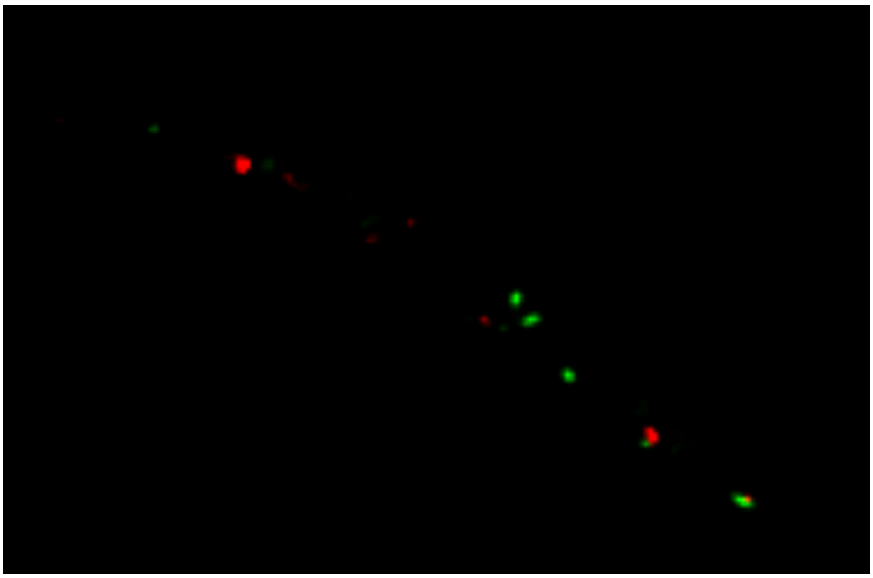

Movie S2. Time-resolved colocalization of *Bs*FliM-CFP and *Bs*FlhG-YFP in *B. subtilis* was monitored by time-lapse fluorescence microscopy over 5 min. We did not observe that stationary FlhG precedes FliM puncta. However, we hardly observed the occurrence of new FliM puncta and therefore can draw no conclusions from this experiment. Images were taken every 10.48 s and are displayed with a frame rate of three frames/s.

Movie S2

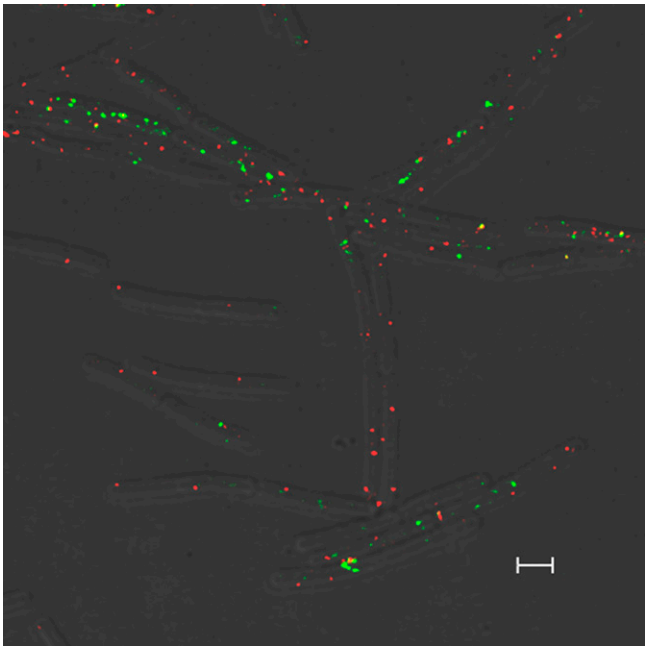

Movie S3. Time-resolved colocalization of *Bs*FliM-CFP and *Bs*FlhG-YFP in *B. subtilis* was monitored by time-lapse fluorescence microscopy over 6.5 min. Images were acquired every 20.33 s and are displayed with a frame rate of three frames/s.

Movie S3

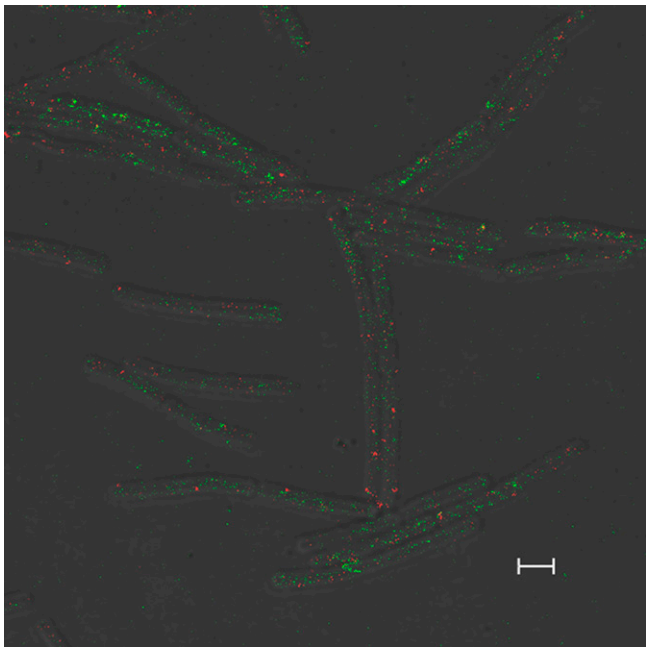

Movie S4. The original data of Movie S3 without deconvolution. Specifications are as stated for Movie S3.

Movie S4